Thermal Stability and Proton Conductivity of Rare Earth Orthophosphate Hydrates

Anfimova, Tatiana; Li, Qingfeng; Jensen, Jens Oluf; Bjerrum, Niels J.

Published in:
International Journal of Electrochemical Science

Publication date:
2014

Document Version
Publisher's PDF, also known as Version of record

Int. J. Electrochem. Sci., 9 **(2014)** 2285 - 2300

International Journal of
ELECTROCHEMICAL
SCIENCE
www.electrochemsci.org

Thermal Stability and Proton Conductivity of Rare Earth Orthophosphate Hydrates

Tatiana Anfimova, Qingfeng Li[*]*, Jens Oluf Jensen, Niels J. Bjerrum*

Section of Proton Conductors, Department of Energy Conversion and Storage, Technical University of Denmark, Kemitorvet 207, 2800 Kgs. Lyngby, Denmark
[*]E-mail: qfli@dtu.dk

Received: 25 October 2013 / *Accepted:* 21 January 2014 / *Published:* 2 March 2014

Hydrated orthophosphate powders of three rare earth metals, lanthanum, neodymium and gadolinium, were prepared and studied as potential proton conducting materials for intermediate temperature electrochemical applications. The phosphates undergo a transformation from the rhabdophane structure to the monazite structure upon dehydration. The thermal stability of the hydrate is studied and found to contain water of two types, physically adsorbed and structurally bound hydrate water. The adsorbed water is correlated to the specific surface area and can be reversibly recovered when dehydrated as long as the rhabdophane structure is preserved. The bound hydrate water is accommodated in the rhabdophane structure and is stable at temperatures of up to 650 ^{o}C. The thermal stability of the hydrate water and the phosphate structure are of significance for the proton conductivity. The $LaPO_4 \cdot 0.6H_2O$ and $NdPO_4 \cdot 0.5H_2O$ exhibited the structure dependence of the proton conductivity while the $GdPO_4 \cdot 0.5H_2O$ showed a large effect of the phosphate morphology.

Keywords: Rare earth phosphates hydrates; Proton conductivity; Impedance spectroscopy; Intermediate temperature fuel cells; Electrolysis

1. INTRODUCTION

Rare earth metal phosphates have been of particular interest to the potential applications in fuel cells, gas sensors and ceramic membranes due to their superior thermal and chemical stability. Recent research has been devoted to exploration of the proton conductivity as potential electrolyte materials for intermediate temperature fuel cells and other electrochemical systems [1,2]. The rare earth metal phosphates exist in nature as monoclinic monazite and tetragonal xenotime. The formula is in both cases MPO_4, but monazite preferentially incorporates mixtures of larger rare earth elements from La to Gd, while the tetragonal xenotime (MPO_4) tends to incorporate the smaller rare earth elements,

typically Y [3]. In their hydrated form ($MPO_4 \cdot nH_2O$) with a typical stoichiometry of $n < 3$, the phosphates adopt the hexagonal rhabdophane crystal structure. See figure 1.

At temperatures above 500 ^oC, the proton conductivity of the monazite form is found to be in a low range of 10^{-7} to 10^{-10} S/cm [4,5]. To explain the proton transfer in the monazite structure, e.g. $LaPO_4$, a sequential intertetrahedral proton transfer mechanism has been proposed [6]. Introduction of an acceptor substituent with a suitable ionic radius can significantly enhance the proton conductivity. Among the investigated alkaline earth metals, particularly strontium [7] has this effect in a concentration of 1 to 5 mol. %. However, this also results in some degree of electronic conduction a high temperature [8-10].

Most work on proton conductivity has been carried out on rare earth metal orthophosphates with the monazite structure. Chemically, rare earth metal phosphates show tendency of forming compounds of high complexity and with high phosphorus contents. This can be achieved by sharing the corner oxygen atom with the adjacent PO_4 tetrahedra. For example, in the La_2O_3-P_2O_5 binary phase system, condensed phosphates of $La(PO_3)_3$ and LaP_5O_{14} are well known [11]. Recent efforts are being made to explore the proton conduction in these polyphopsphates. Ray et al. [12] prepared LaP_3O_9 and CeP_3O_9 glasses and obtained conductivities of $10^{-7.5}$ – 10^{-6} S/cm at 400^oC. Similar to the orthophosphates, when lanthanum ions were partially substituted by divalent metal ions such as Ca^{2+}, Sr^{2+} and Ba^{2+} [13,14], higher proton conductivities were reported for the polyphosphates, indicating that the substitution lead to proton dissolution into the material and induced protonic conduction. The highest conductivity of 5×10^{-4} Scm^{-1} was reported for 3 mol% Sr-doped LaP_3O_9 at 427 °C [15]. Further condensed phosphates in form of e.g. LaP_5O_{14} are believed to provide low energy avenues for proton transport and therefore lead to enhanced conductivity [2,16,17].

These condensed phosphates are well known to undergo phase transformations with temperature. For example, during the synthesis by solution routes, Jørgensen et al. [18] found that the residues of hydrogen phosphates in form of adsorbed surface species led to formation of lanthanum metaphosphate (LaP_3O_9) upon heating to above 600 ^oC. The LaP_3O_9, in turn, decomposed to $LaPO_4$ with loss of P_2O_5 at temperatures above 877 ^oC and even transformed to an amorphous phase.

Another type of structural transformation of rare earth phosphates is between the monoclinic monazite (MPO_4) and hexagonal rhabdophane ($MPO_4 \cdot nH_2O$) through hydration and dehydration[19]. The naturally occurring rhabdophane is of a significant variety of the rare earth metal compositions [20], where the water molecule is accommodated in the "zeolitic" channels of the structure [21]. This type of phosphate structures is metastable. It dehydrates when heated to elevated temperatures and further transform to the monazite structure at even higher temperatures. The presence and stability of the hydrate water in the rhabdophane phosphates are of particular interest from the proton conductivity point of view, to which the present work is devoted.

2. EXPERIMENTAL

2.1. Synthesis.

Lanthanide phosphate hydrates were prepared using La_2O_3 (Sigma-Aldrich 99.99 %), Nd_2O_3 (Sigma-Aldrich 99.9 %) and Gd_2O_3 (Megon 99.99 %) by a wet precipitation method. The individual

oxide was added into a 0.6 M aqueous H_3PO_4 solution and the mixture was heated to 150 °C and kept for 3 hours under constant stirring. The resulting precipitates were slowly cooled down to room temperature and then filtered from the solution with following washing of the precipitate.

2.2. Characterization

The density of the powders was measured by a Micromeritics AccuPyc 1330. The BET measurements were carried out by a Micrometrics Gemini Surface Area Analyzer, working at 77 K after degassing the powder at 300 °C. The BET area was calculated by using the experimental points between 0.05 and 0.25 bar of the N_2 partial pressure. Powder X-ray diffraction (XRD) patterns of the dried particles were recorded from 3° to 100º with a Huber D670 diffractometer with CuKα radiation (λ=1.54056). The crystalline phases were determined from the comparison of registered patterns with the Inorganic Crystal Structure Database (ICSD) Version 1.7.2.

For the Fourier transform infrared spectroscopy (FT-IR), powder sample spectra were recorded using a Perkin-Elmer VATR TWO spectrometer in the range 450 - 4000 cm^{-1} with a resolution of 4 cm^{-1} under ambient atmosphere and at room temperature. The spectra were integrated using the Spectrum software.

Thermogravimetric analyses (TGA, DTA) were performed on a Netzsch STA 409 PC. Air, argon and 5 vol. % of hydrogen in nitrogen as a reducing atmosphere were used as purge gasses and the powder samples were heated with a heating rate of 10 K/min.

2.3. Conductivity measurements

The phosphate powder was pressed (10 tons) into a disc of a diameter 1 - 3 cm and a thickness of about 2 mm. The disc was on each side coated with a thin layer of silver paste (LOCTITE® 3863 from Henkel Co.), onto which a gold mesh was placed as electrical lead. The assembly was held together by two discs of porous SiC and contained in a stainless steel tube with an inlet and an outlet for an air flow. Water was added through an evaporator to achieve a certain water partial pressure in the air flow. Impedance spectra of the samples were measured by a Princeton Potentiostat Versa Stat 3 equipped with a Versa Studio software. The frequency range was between 0.01 Hz and 1 MHz and the temperature was varied from 120 °C and up to 250 °C. The conductivity (σ) of the disc was calculated from the measured resistance (R) by using the following equation where L is the thickness and A is the cross-sectional area of the disc, respectively:

$$\sigma = L/RA$$

2.4. Structural modeling

The structural modeling was made by the Atoms V6.3 software using X-ray diffraction data. The software calculates positions of atoms and bonds distances from the X-ray diffraction pattern automatically.

3. RESULTS AND DISCUSSIONS

3.1. Structural modeling

Figure 1 shows the structure for neodymium phosphates as calculated from the XRD data.

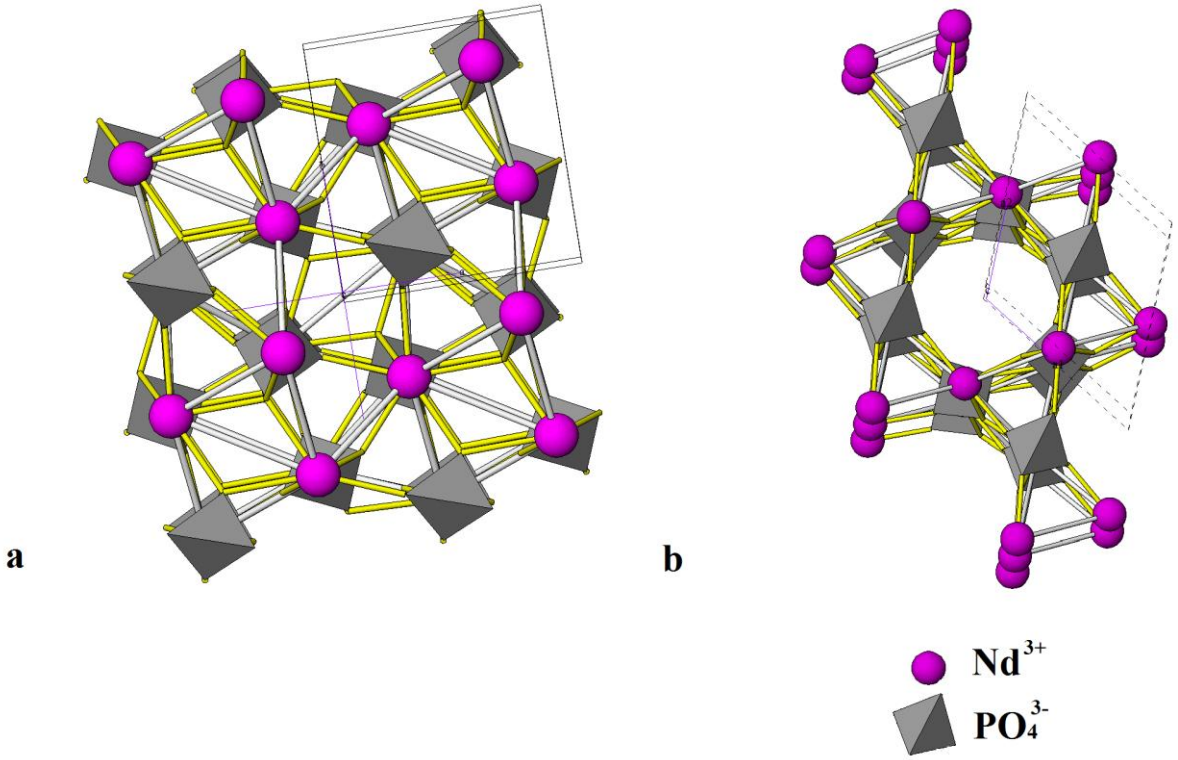

Figure 1. View of the $NdPO_4$ structure along the c-axis. a) The monoclinic monazite structure and b) the hexagonal rhabdophane structure with channels that can accommodate water (not shown).

The crystal structure of $NdPO_4$ as seen along the c-axis is shown in Fig.1a. It consists of isolated PO_4 tetrahedra, which are held together by Nd^{3+} cations. Each Nd^{3+} cation is surrounded by nine oxygen ions. The crystal structure of the hydrated form of $NdPO_4$ (rhabdophane) seen along the c-axis is shown in Fig.1b. The location of water molecules is suggested by use of geometrical considerations. According to Mooney [21], adjacent sites are only 2.15 Å apart along the hexagonal axis and are assumed to preclude the occupancy of every unit cell by a water molecule. At the maximum, only half of the sites can be occupied, or in other words, there can be only one and a half molecules of water per unit cell. Therefore, if water is present in the crystal structure there should be no more than half a molecule per rare earth metal atom. The location of water molecules is only possible on the 6_2 axes, in rows. The existence of such unoccupied spaces explains the relatively low density of the hexagonal isomorph as compared to the monoclinic monazite (see Table 1). Mooney [21] also suggested that the crystal structure of $NdPO_4 \cdot nH_2O$ may be stabilized by the presence of water in the interstices. These sites could accommodate a neutral molecule of water or even ions of a suitable size if the charges could be compensated in some ways. An ionic radius depends on the

coordination number, spin state and other parameters. The effective ionic radius of trivalent lanthanides in the eight and nine-fold coordination are given in Table 1. In the table are also listed the lattice parameters of these phosphates, which are also plotted as a function of the ionic radius in Fig.2.

Table 1. Crystal radius of trivalent lanthanide ions in eight and nine coordination as compared to the unit cell dimension of monazite and rhabdophane orthophosphates. Densities are listed too.

Name	Effective Ionic Radius of M^{3+} [22,23], nm		Unit Cell Dimension, nm		Density, g/sm^3	
	In eight coordination	In nine coordination	a	c	Theoretical	Experimental (this work)
$LaPO_4$	-	0.1216 [24]	0.6825	0.6482	5.11	-
$LaPO_4 \cdot nH_2O$	0.1160 [21]	-	0.7081	0.6468	4.15	4.13
$NdPO_4$	-	0.1163[25]	0.6732	0.6383	5.49	-
$NdPO_4 \cdot nH_2O$	0.1109 [21]	-	0.698	0.638	4.45	4.02
$GdPO_4$	-	0.1107 [26]	0.6621	0.631	6.06	-
$GdPO_4 \cdot nH_2O$	0.1053 [27]	-	0.6906	0.6326	5.05	4.68

Fig.2 illustrates differences in unit cell parameters both for monazite (monoclinic) and rhabdophane (hexagonal) structures as well as gadolinium contraction. It can be seen from the figure that the parameters a and c of the unit cell are larger for the rhabdophane structure than for that of the monazite.

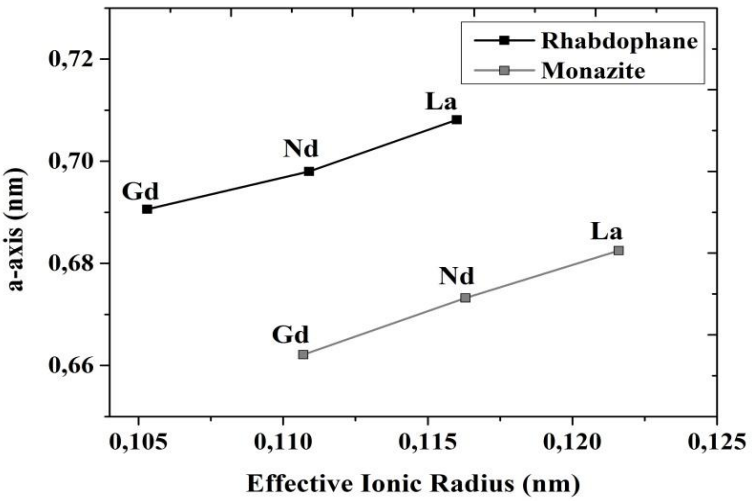

A

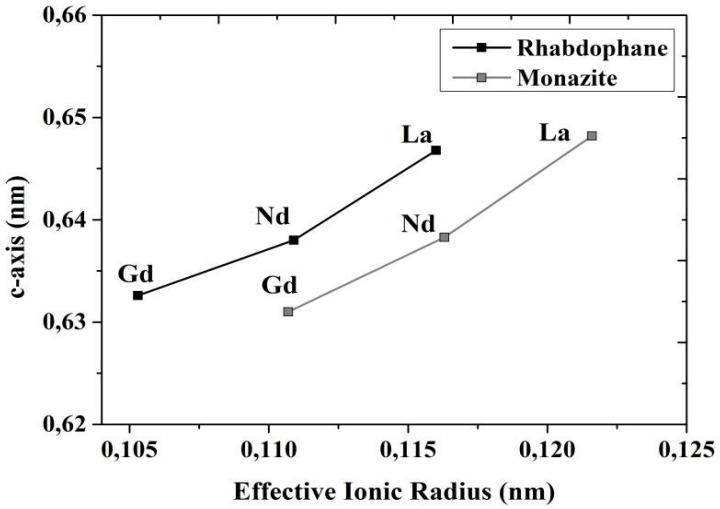

B

Figure 2. a-axes (a) and c-axes (b) of the rhabdophane $MPO_4 \cdot nH_2O$ and monazite MPO_4 unit cells plotted against effective ionic radius of the corresponding lanthanide.

This can be explained by channels present in the rhabdophane structure, which is accommodating water molecules. When water molecules are leaving the channels during the heating, the rhabdophane type unit cells contract in order to compensate the open space and transform into the more dense monazite type structure.

This process is believed to be slow and energy consuming. After such a transformation it would be difficult for the water molecules to be introduced into unit cells again because of the contraction.

3.2. XRD

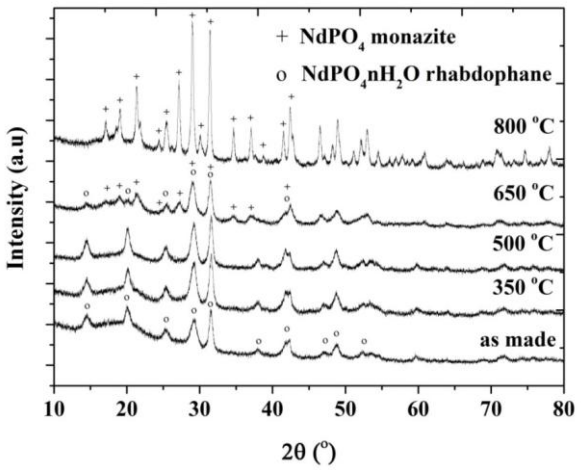

Figure 3. X-ray diffraction patterns of $NdPO_4 \cdot nH_2O$ powders as prepared and heat treated at different temperatures each for a period of 6 hours. Indexing for rhabdophane [21] and monazite [25] structures is indicated in the figure.

The hexagonal structure is the low-temperature phase stabilized by hydrate water. The assigned peaks are marked on the X-ray diffraction patterns of unheated samples (Fig. 3, open circles). Wide peaks are a typical feature for $MPO_4 \cdot nH_2O$ powders and it is an indication of low crystallinity of the unheated samples. The crystallinity is increasing slightly with temperature until the transition temperature. No presence of the monazite phase (crosses) was observed in the X-ray diffraction patterns of $NdPO_4 \cdot nH_2O$ after the heat-treatments at below 650 ^oC. The X-ray diffraction pattern of the powder heat-treated at 650 ^oC showed the presence of both rhabdophane and monazite structures. Finally at 800 ^oC the crystalline phase of the rhabdophane disappeared. The X-ray diffraction patterns of the $LaPO_4 \cdot nH_2O$ and $GdPO_4 \cdot nH_2O$ showed the same behavior. It is noted that for the $LaPO_4 \cdot nH_2O$ powder by heat treatment at temperatures up to 350 ^oC contained three additional peaks in the 2θ region from 10 to 30^o, which were not recognized by the data base and suggested to be due to contamination by the churchite phase ($LaPO_4 \cdot 2H_2O$).

3.3. FT-IR spectra

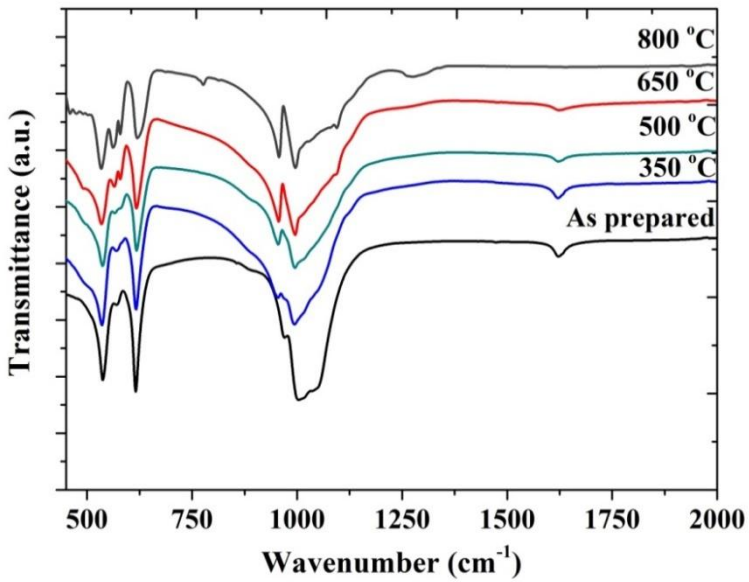

Figure 4. Typical FT-IR spectra of neodymium phosphate $NdPO_4 \cdot nH_2O$. Temperatures of heat treatment are indicated

Infrared spectroscopy has proved to be an important tool for determining the different structures of rare earth phosphates. The space group of the hexagonal form of the $MPO_4 \cdot nH_2O$ is *P*6222 [21]. This space group provides sets of three-fold sites with the point symmetry D_2 for the metal and phosphate ions, and six-fold sites with the point symmetry C_2 for phosphates [28]. The nature of vibrations of the phosphate group was described by Assaaoudi [29] for the wheinshenkite-type compounds and for the rhabdophane-type compounds. The band at 1631 cm^{-1} was assigned to the hydration water of the hexagonal $MPO_4 \cdot nH_2O$ [30]. FT-IR spectra in Fig.4 shows a decrease of this

band indicating loss of water in $NdPO_4 \cdot nH_2O$. Similar behaviors were observed for the other two phosphates. The characteristic water band can be observed at temperatures up to 650 ^oC. Thus together with X-ray diffraction pattern studies this result proves that the rhabdophane phase can be present in the structure at temperatures up to 650 ^oC and partly recoverable during the cooling process under ambient atmosphere by accommodation of water molecules into the structure. Another interesting region is in the range of 500 - 600 cm^{-1} where peaks connected to the vibration of PO_4 groups are located. The presence of three clear peaks on the FT-IR spectra for the sample heat threated at 650 ^oC is characteristic of the vibrations of phosphate groups in the monoclinic structure of monazite structured $NdPO_4$ and assumed to result from the distortion of the tetrahedral phosphate groups in the nine fold coordinated Nd atoms [25].

3.4. TG/DT Analyses

3.4.1. Thermal stability in air

The samples were studied by DTA/TGA analyses in order to determine the amount of residual water in the powders. Using the heating program, powders were heated up to 800 °C with a constant heating speed of 10 K/min in air and the main mass losses caused by removal of water from the initial powders were observed until 500 °C (see Table. 2). The TGA/DTA results are shown in Fig.5.

The occurring weight loss could be divided in three regions. In the first region below 200 ˚C, a weight loss of about 3.5-4 wt% accompanied by an endothermic peak with a maximum at about 100-140 ˚C is assumed to be associated with the water adsorbed on the surface (see Table 2) during the storage in air. It is likely that the amount of the adsorbed water depends on the surface area of powders. Powders of lanthanum and neodymium phosphates have higher surface areas than that of gadolinium phosphates (see Table 2), which might be explained by differences in the particle size of initial oxides and therefore the obtained phosphates. It must be taken into account that the surface area affects the content of nonstoichiometric water and therefore most likely the conductivity of the phosphates too. This is clearly seen for the $GdPO_4 \cdot nH_2O$ sample as the powder has a low surface area and hence low water adsorption.

The second event between 200 - 500 ^oC with a corresponding endothermic maximum at around 200 - 250 ^oC is assigned to the dehydration of the hexagonal phase ($MPO_4 \cdot nH_2O$). An important weight loss was registered before 300 ^oC which continued at temperatures up to 450 ^oC. The total weight loss of this event was found to be dependent on the synthesis conditions and corresponded to a hydration ratio, n, of around 0.5 for the phosphates. The additional endothermic peak for the $LaPO_4 \cdot nH_2O$ sample in the 300-350 ^oC region was not recognized in the neodymium and gadolinium phosphates, most likely due to the presence of phase impurities as revealed by X-ray diffraction analysis.

The last event above 450 ^oC with an exothermic peak at about 500 ^oC was not accompanied by significant mass losses and presumed to represent the beginning of transformation from the rhabdophane to the monazite structure. This phase transition was supported by the X-ray diffraction analysis in Fig. 3 and FT-IR in Fig. 4. The structural differences between these two phases have been

described previously. The temperature of this transition is higher in this case than previously reported by others [30], which can be explained by the fast heating rate (10 K/min). The exact temperature of the structural transition is strongly depending on initial conditions of the synthesis and the amount of nonstoichiometric water.

The results of the TGA measurements are summarized in Table 2. It is clear that the first TGA event at up to 150 °C corresponds to the release of adsorbed water. This part of water loss is of surface nature and dependent on the specific surface area of the phosphates not including the channels. The second event in the temperature region from 200 to 500 °C is due to the de-hydration of the rhabdophane phase.

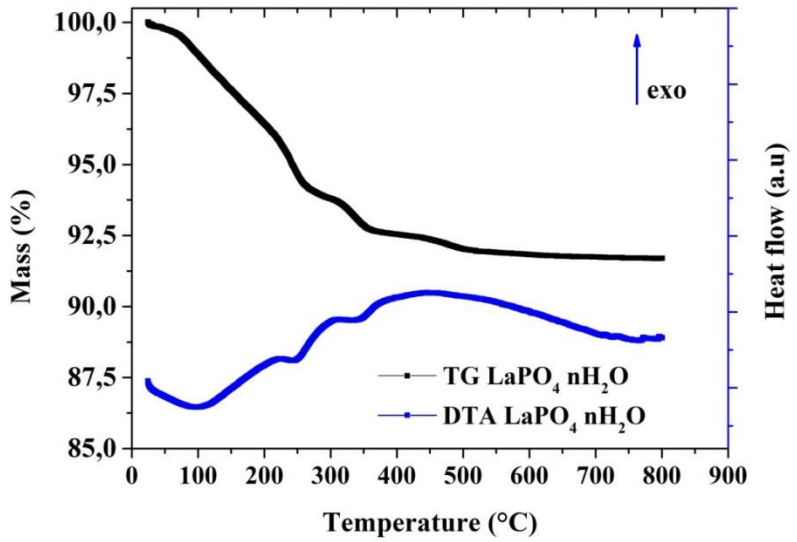

(a)

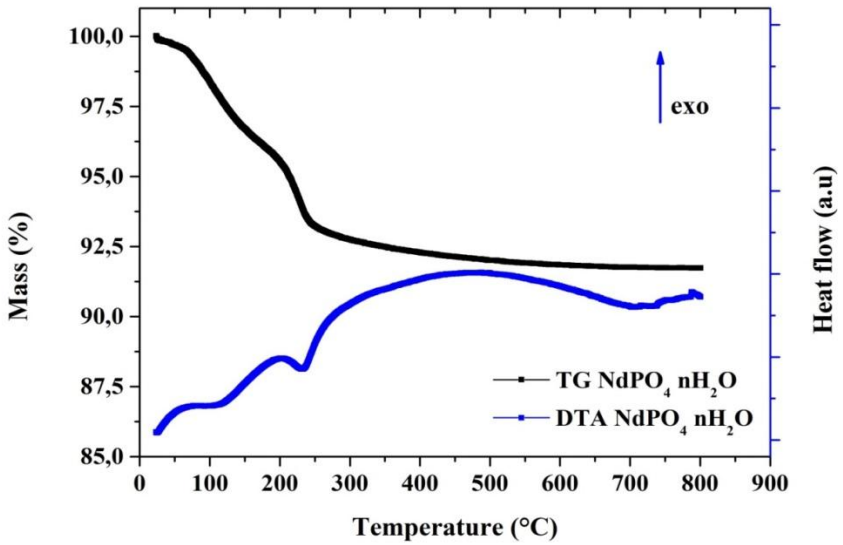

(b)

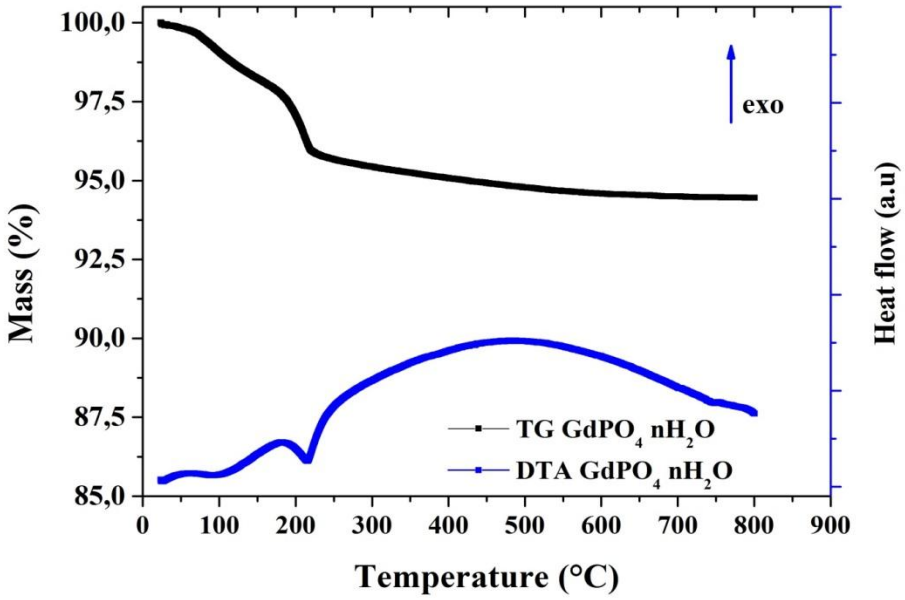

(c)

Figure 5. TGA (solid black) and DTA (solid blue) analyses for powders of (a) $LaPO_4 \cdot nH_2O$, (b) $NdPO_4 \cdot nH_2O$, and (c) $GdPO_4 \cdot nH_2O$ in ambient atmosphere and at a heating rate of 10 K/min.

Table 2. Water losses determined by TGA assuming that the weight loss can be assigned solely to loss of water.

Samples	BET, m^2/g (this work)	As prepared phosphates		Heat treated at 150 °C		Heat treated at 500 °C	
		Water losses %	Calculated water content	Water losses %	Calculated water content	Water losses %	Calculated water content
$LaPO_4 \cdot nH_2O$	78	8.3	1.2	4.5	0.6	1.1	0.1
$NdPO_4 \cdot nH_2O$	82	8.2	1.2	3.3	0.5	0.9	0.1
$GdPO_4 \cdot nH_2O$	25	5.5	0.8	3.1	0.5	1.2	0.2

The value of the hydration water, n, was estimated and found to be $LaPO_4 \cdot 0.6H_2O$, $NdPO_4 \cdot 0.5H_2O$, $GdPO_4 \cdot 0.5H_2O$. This part of water loss should be reversible to a great extent, as there is no structural transformation from rhabdophane to monazite involved. This implies that the dehydration of the rhabdophane phosphates within this temperature region can be restored if water is present in the vapor phase. Combination of the X-ray diffraction data (Fig.3) with TGA/DTA results led to the conclusion that in the temperature region from 500 to 800 ^oC, a structural transformation from the rhabdophane to monazite occurs. As proposed by Lucas et al. [30], the following reaction takes place:

$MPO_4 \cdot nH_2O$ (hexagonal) ↔ MPO_4 (hexagonal) + $nH_2O_{(gas)}$

followed by:

MPO_4 (hexagonal) → MPO_4 (monocline)

This is accompanied by the further loss associated with condensation of orthophosphates to pyro- or higher phosphates. As discussed in the crystal structures of phosphates above, the rhabdophane-to-monazite transformation resulted in the unit cell contraction and therefore irreversible dehydration.

3.4.2. Thermal stability under reducing and inert atmospheres

Further investigation was made by varying heating programs under different atmospheres in order to understand the behavior of water molecules in the crystal structures. In terms of hydrolytic stability of the phosphates and their conductivities in the temperature range of 200 - 400 °C was of particular importance for applications in intermediate temperature fuel cells and other electrochemical systems. During the experiment under a reducing atmosphere (5 vol. % of hydrogen in nitrogen), the powders were heated at a rate of 2 K/min to 150 °C in order to remove the adsorbed water. The samples were then cooled to 100 °C and the TGA curves were recorded from 100 to 400 °C. The typical result for the $GdPO_4 \cdot nH_2O$ powder is presented in Fig. 6a. Only one endothermic peak is present at 170-230 ^oC, attributable to the dehydration of the rhabdophane phase. The total weight loss is found to be 3.1 wt %, corresponding to a hydration number, n, of 0.5, in good agreement with the result estimated by Mooney [21].

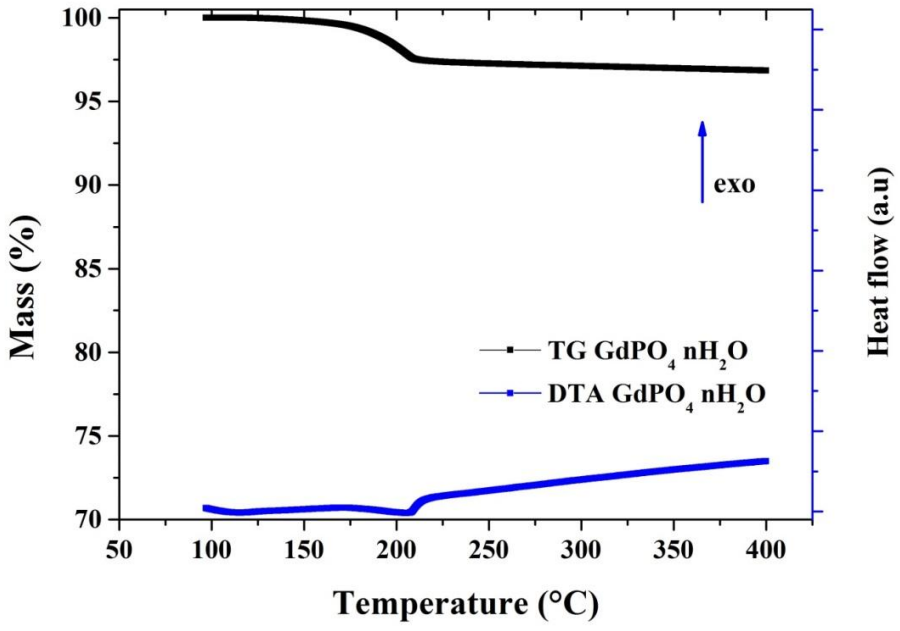

(a)

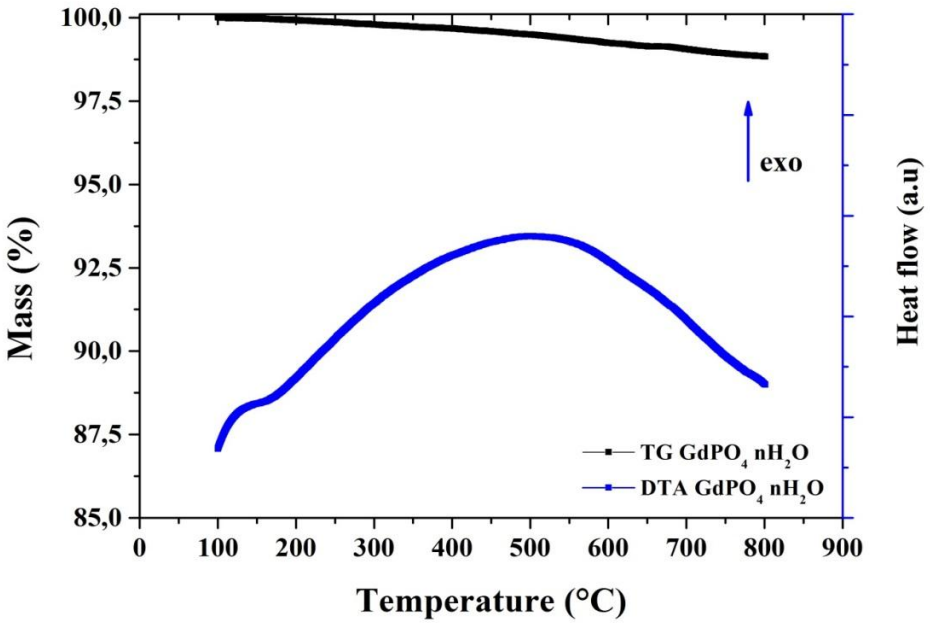

(b)

Figure 6. TGA (black line) and DTA (blue line) analyses for $GdPO_4 \cdot nH_2O$. (a) under a reducing atmosphere (5 vol% H_2 in N_2) in the temperature range of 100 to 400 ^oC and (b) under an inert (argon) atmosphere in the range of 100 to 800 ^oC.

During the experiment in the inert atmosphere the powders were first heated at a heating speed of 2 K/min up to 500 °C. The samples were then cooled to 100 °C and TGA was recorded from 100 to 800 °C, as shown in Fig. 6b. The presence of remaining water after being heated at up to 500 °C gave a further weight loss of about 1%, accompanied with a small endothermic peak. The water loss in this temperature range indicates the slow phase transition from the rhabdophane to monazite structure. This fact is in a good agreement with the X-ray diffraction and FT-IR analyses, which showed the presence of the rhabdophane phase at temperatures of up to 650 ^oC. Similar behaviors were observed for the other two phosphates, though not shown in the figure. The presence of dehydration peaks for the three $MPO_4 \cdot nH_2O$ suggests a similar dehydration process for the phosphates under varied atmospheres. The binding of water molecules in the rhabdophane structure is very strong, as expected from the zeolitic structures of the phosphates. The chemical and thermal stability of rhabdophane phosphates, or in other words, the associated water molecules, are of special interest for the proton conductivity.

3.5. Conductivity

The typical impedance plots are shown in Fig.7a for $NdPO_4 \cdot nH_2O$. The plots consist of two arcs: one located at high frequencies and the other, which is normally uncompleted, at low frequencies. The resistance of samples was found by fitting the first arc into semicircle with a diameter, which was taken as the bulk resistance of the sample. The conductivity of three phosphates is calculated from the resistance, and shown in Fig.7b. Additionally shown in the figure is the theoretical calculation on the

basis of the DFT calculations for lanthanum monazite by Yu et al. [6]. The measured conductivity of $LaPO_4 \cdot nH_2O$ was slightly lower but in a reasonable range close to the theoretic estimation of the proton conductivity of the monazite phosphates. The activation energy was found to be 0.61 eV for $LaPO_4 \cdot nH_2O$, close to 0.8 eV, the value predicted for monazite by Yu et al. For neodymium phosphates the conductivity is about one order of magnitude higher than that of $LaPO_4 \cdot nH_2O$ with a leveling off at temperatures above 230 °C.

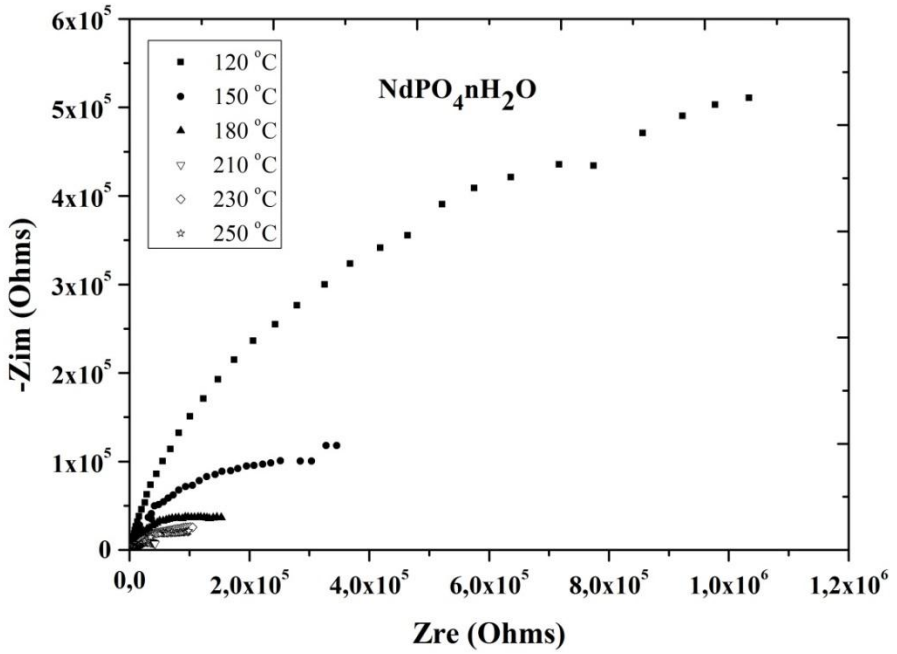

(a)

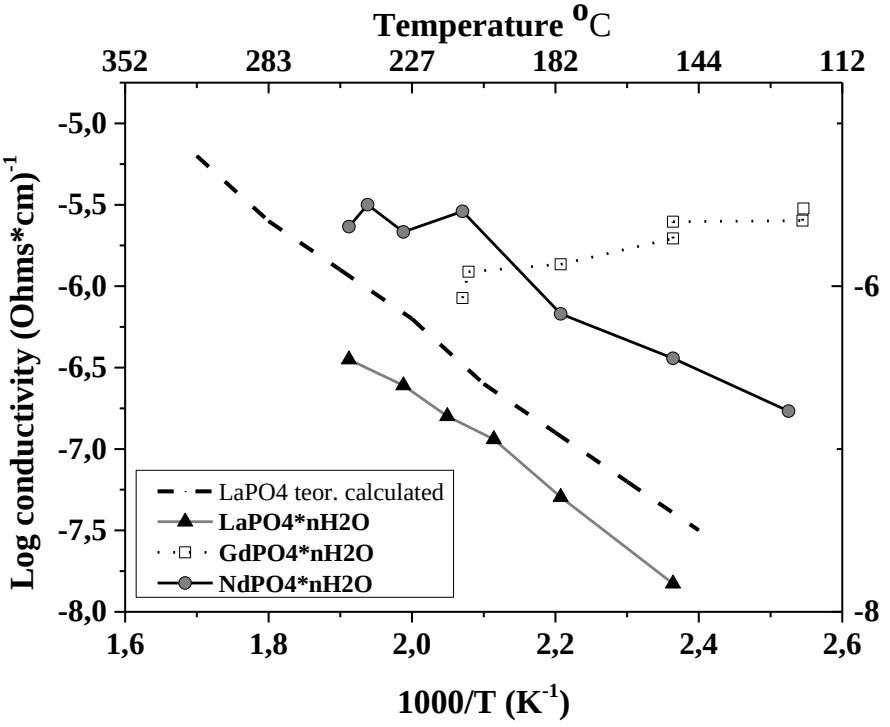

(b)

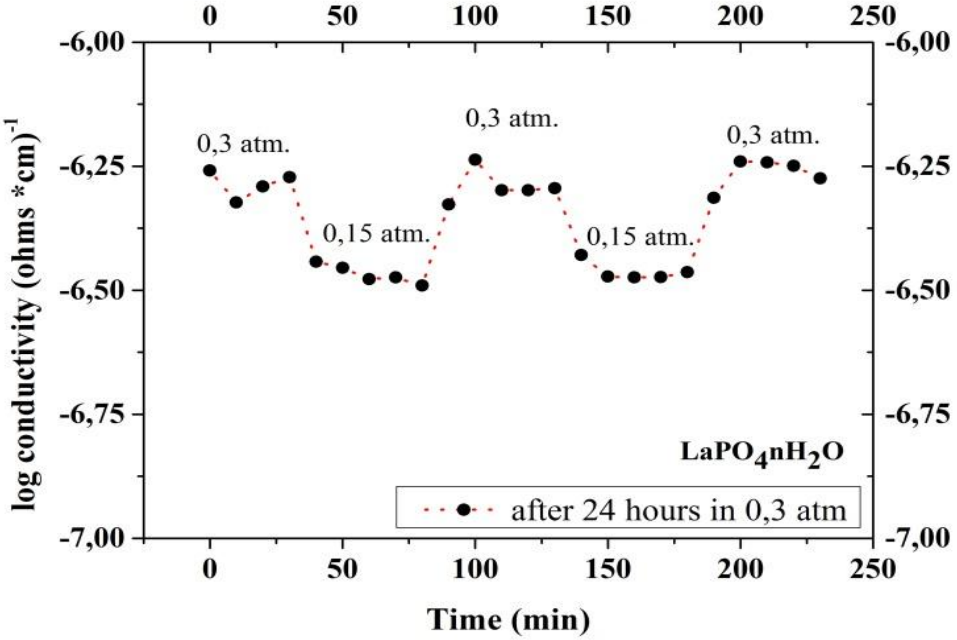

(c)

Figure 7. (a) Typical Nyquist plot for $NdPO_4 \cdot nH_2O$; (b) Conductivity of $MPO_4 \cdot nH_2O$ (where M = La, Nd and Gd) measured under a water partial pressure of P_{H_2O} = 0,15 atm as compared with literature data for $LaPO_4$ [6]; (b) Conductivity of the three phosphates; (c) Stability of the conductivity under the humidity cycling between P_{H_2O}=0.3 atm and P_{H_2O}= 0.15 atm

The average activation energy over the entire studied temperature range from room to 250 °C was found to be about 0.41 eV. The higher conductivity and lower activation energy for $NdPO_4 \cdot nH_2O$, as compared to $LaPO_4 \cdot nH_2O$, is likely connected to the contraction of unit cells, which would shorten the interatomic distance and therefore facilitate the proton conduction. In the low temperature range, the conductivity of $GdPO_4 \cdot nH_2O$ followed the same trend, i.e. much higher conductivity than that of the other two phosphates. When the temperature was further increased, the conductivity remained unchanged or even decreased. As seen from the BET measurements, the as prepared $GdPO_4 \cdot nH_2O$ powder had a much smaller specific surface area, which in turn resulted in less water adsorption. Indeed the TGA data confirmed a lower water loss of $GdPO_4 \cdot nH_2O$, compared to its analogues (see Table 2). This may partly explain the unusual temperature dependence of the conductivity.

Further investigations were made on $LaPO_4 \cdot nH_2O$ for stability evaluation of the conductivity. Fig. 7c shows the result during an overall period of 28 hours. The sample was kept at 250 °C under P_{H_2O} = 0.3 atm for 24 hours. During the period, the conductivity was slightly increased to reach a stable value of 5×10^{-7} S/cm. This value is slightly higher than that (3×10^{-7}) from Fig. 7b, where the water partial pressure was 0.15 atm. The water partial pressure was then cycled from 0.3 to 0.15 atm (3 cycles within 4 hours). The conductivity was decreased to 3×10^{-7} S/cm within 20 minutes and remained stable for the rest time of the first cycle. The water partial pressure was thereafter brought back to 0.3 atm, when the conductivity was completely restored in 20 minutes. The cycling was repeated with very good reproducibility. This is clearly verifying the chemical and the thermal stability of the rhabdophane phosphates and the reversibility of hydration and dehydration within the

temperature and humidity range. The conductivity is however low for any practical applications of this type of materials in fuel cells or other electrochemical systems at intermediate temperatures. Further exploration in forms of composites with other proton conducting materials is in progress [31].

4. CONCLUSIONS

Three hydrated orthophosphates were prepared from La_2O_3, Nd_2O_3 and Gd_2O_3 by wet precipitation in phosphoric acid aqueous solutions. Thermogravimetric analyses in air showed the following compositions of the hydrated orthophosphates: $LaPO_4 \cdot 0.6H_2O$, $NdPO_4 \cdot 0.5H_2O$, $GdPO_4 \cdot 0.5H_2O$. Two types of water were identified in these systems, the physically absorbed and structurally bound water. The absorbed water was of surface nature and correlated to the specific surface area of the phosphates, which could be reversibly recovered when dehydrated at temperatures below 650 °C. The hydrate water molecules were associated with the rhabdophane structure of the phosphates and stable at temperatures of up to 650 ^oC. Above this temperature, dehydration took place with a structural transformation from the hexagonal rbabdophane structure to the monoclinic monazite structure. As a result of the structural contraction the dehydration is irreversible. The thermal stability of the hydrate water and therefore the structure of the phosphates were of significance for the proton conductivity. Among the studied phosphates, $LaPO_4 \cdot nH_2O$ and $NdPO_4 \cdot nH_2O$ exhibited the conductivity and temperature dependence in good agreement with the theoretic estimation for their monazite analogues while the prepared $GdPO_4 \cdot nH_2O$ showed significant effects of the phosphate morphology.

ACKNOWLEDGEMENT
This work has received financial support from the Danish National Research Foundation (the PROCON Center) and the Danish Council for Strategic Research (MEDLYS).

References

1. T. Norby, N. Christiansen, *Solid State Ionics* 77 (1995) 240
2. S. R. Phadkew and J.C. Nino, *J. Am. Ceram. Soc.,* 94 (2011) 1817
3. Y. X. Ni, J. M. Hughes,A. N. Mariano, *Am. Mineral.*, 80 (1995) 21
4. N. Kitamura, K. Amezawa, Y. Tomii, N. Yamamoto, *Solid State Ionics* 162-163 (2003) 161
5. K. Amezawa, Y. Tomii, N. Yamamoto, *Solid State Ionics* 176 (2005) 143
6. R. Yu, L. C. De Jonghe. *J. Phys. Chem., C*, 111 (2007) 11003
7. K. Amezawa, Y. Tomii, N. Yamamoto, *Solid State Ionics* 176 (2005) 135
8. K. Amezawa, H. Maekawa, Y. Tomii, N. Yamamoto, *Solid State Ionics* 145 (2001) 233
9. S. Gallini, M. Hänsel, T. Norby, M.T. Colomer, J.R. Jurado, *Solid State Ionics* 162–163 (2003) 167
10. N. Kitamura, K. Amezawa, Y. Uchimoto, Y. Tomii, T. Hanada and T. Yamamoto, *Solid State Ionics*, 177 (2006) 2369
11. H. D. Park, E.R. Kreidler, *J. Am. Ceram. Soc.*, 67 (1984) 23
12. H. L. Ray, L.C. De Jonghe and R.G. Wang, *ECS Trans.*, 16 (51) (2009) 389
13. K. Amezawa, T. Tomiga, T. Handa, Yamamoto N., Y. Tomii, *J. Am. Ceram. Soc.*, 88 (2005) 3211

14. K. Amezawa, Y. Kitajima, Y. Tomii, N. Yamamoto, M.Widerøe, T. Norby, *Solid State Ionics* 176 (2005) 2867
15. K. Amezawa, Y. Uchimoto,Y. Tomii. *Solid State Ionics* 177 (2006) 2407
16. A. Unemoto, K. Amezawa, T. Kawada, *J. Electrochem. ceram.*, 29 (2012) 29
17. 17. I. Hammas, K. Horchani-Naifer, M, Ferid, *J. Rare Earths*, 28 (2010) 321
18. S. Jørgensen, J. A. Horst, O. Dyrlie, Y. Larring, H. Ræder, T. Norby, *Surf. Interface Anal.*, 34 (2002) 306
19. S. Lucas, E. Champion, D. Bernache-Assollant, G. Leroy, *J. Solid State Chem.*, 177 (2004) 1302
20. J. F. W. Bowles and D. J. Morgan, *Mineral. Mag.*, 48 (1984) 146
21. R. C. L. Mooney, *Acta Crystallogr.*, 3 (1950) 337
22. R.D. Shannon. *Acta Crystallogr.*, A32 (1976) 751
23. R. Dronskowski, *Computational Chemistry of Solid State Materials*. WILEY-VCH, Weinheim (2005)
24. D. F. Mullica, W. O. Milligan, D.A. Grossie, G.W. Beall, L.A. Boatner, *Inorg. Chim. Acta* 95 (1984) 231
25. D.F. Mullica, D.A Grossie, L.A Boatner. *J. Solid State Chem.*, 57 (1985) 71
26. D.F. Mullica, D.A. Grossie, L.A. Boatner, *Inorg. Chim. Acta* 109 (1985) 105
27. B. Scheetz, D. Pfoertsch, L. Zellmer, D. Smith, Penn. State. Univ., *JCPDS Grant-in-Aid Report*, (1987)
28. R.S. Halford, *J. Chem. Phys.* 14 (1948) 8
29. H. Assaaoudi, A. Ennaciri, A. Rulmont. *Vibrat. Spectr*. 25 (2001) 81
30. S. Lucas, E. Champion, D. Bregiroux, D. Bernache-Assollant, G. Leroy , *J. Solid State Chem.*, 177 (2004) 1312
31. T. Anfimova, N.J. Bjerrum, Q. Li. *Adv. Mater. Research* 699 (2013) 398